Thermoelectric Efficiency in Nanojunctions: A Comparison between Atomic Junctions and Molecular Junctions

ARTICLE *in* ACS NANO · NOVEMBER 2009

Impact Factor: 12.88 · DOI: 10.1021/nn900986r · Source: PubMed

3 AUTHORS, INCLUDING:

Yushen Liu
Changshu Institute of Technology
57 PUBLICATIONS **420** CITATIONS
SEE PROFILE

Yu-Chang Chen
National Chiao Tung University
37 PUBLICATIONS **884** CITATIONS
SEE PROFILE

Thermoelectric Efficiency in Nanojunctions: A Comparison between Atomic Junctions and Molecular Junctions

Yu-Shen Liu, Yi-Ren Chen, and Yu-Chang Chen*

Department of Electrophysics, National Chiao Tung University, 1001 Ta Hsueh Road, Hsinchu 30010, Taiwan

ABSTRACT Using first-principles approaches, we investigate the thermoelectric efficiency, characterized by the figure of merit ZT, in metallic atomic junctions and insulating molecular junctions. To gain insight into the properties of ZT, an analytical theory is also developed to study the dependence of ZT on lengths (l) and temperatures (T). The theory considers the combined heat current carried by electrons and phonons. We observe a characteristic temperature: $T_0 = (\beta/\gamma(l))^{1/2}$. When $T \ll T_0$, the electronic heat current dominates the combined heat current and ZT $\propto T^2$. When $T \gg T_0$, the phononic heat current dominates the combined heat current and ZT tends to a saturation value. Moreover, the metallic atomic junctions and the insulating molecular junctions have opposite trend for the dependence of ZT on lengths, that is, ZT increases as the length increases for aluminum atomic junctions, while ZT decreases as the length increases for alkanethiol molecular junctions.

KEYWORDS: thermoelectricity · Seebeck coefficient · thermoelectric figure of merit · electronic heat conductance · phononic heat conductance · atomic junction · single-molecule junction · density functional theory

Recent experiments have demonstrated the capability of measuring the Seebeck coefficients in atomic and molecular junctions.[1−4] These experiments have inspired rapid theoretical development in the thermoelectric properties of nanojunctions.[5−15] This interest is partially motivated by the possible application of such nanojunctions in thermoelectric devices and partially by the desire to understand the thermoelectric properties found in atomic-sized junctions. Thermoelectric nanodevices can be considered as new style devices which can be integrated into chip sets in order to assist the stability of devices by converting the accumulated waste heat into usable electric energy. As the Seebeck coefficients are relevant not only to the magnitude but also to the slope of density of states (DOSs), they can reveal more detailed information about the electronic structures of the nanostructured objects bridging the nanojunctions beyond what the conductance measurements can provide. The Seebeck coefficient has been used to explore the electronic structures of molecular junctions using functional substitutions for the bridging molecules.[2,3,14] The gate field has been theoretically proposed as a means of modulating the conduction mechanism between p-type [in which the Fermi energy is closer to the highest occupied molecular orbital (HOMO)] and n-type [in which the Fermi energy is closer to the lowest unoccupied molecular orbital (LUMO)] *via* the sign of the Seebeck coefficient.[6,7,14] Although much research has been devoted to the study of Seebeck coefficients, little is known about the efficiency of energy conversion in nanojunctions.[10] As such, the objective of this research is to provide deeper insights into the thermoelectric efficiency, usually characterized as the thermoelectric figure of merit ZT. This study has considered the combined heat currents, including the electronic and phononic heat currents.

Thermoelectric nanojunctions consist of a nanostructured object sandwiched between source−drain electrodes serving as independent electron reservoirs with distinct chemical potentials $\mu_{L(R)}$ and independent temperature reservoirs with distinct temperatures $T_{L(R)}$. The thermoelectric figure of merit ZT depends on the following several physical factors: the Seebeck coefficient (S), the electric conductance (σ), the electronic heat conductance (κ_{el}), and the phononic heat conductance (κ_{ph}). The thermoelectric efficiency in the nanoscale junctions can thus be described by the dimensionless thermoelectric figure of merit presented as[11]

$$ZT = \frac{S^2\sigma}{\kappa_{el} + \kappa_{ph}}T \qquad (1)$$

where T is the average temperature in the source−drain electrodes. When ZT tends to

*Address correspondence to yuchangchen@mail.nctu.edu.tw.

Received for review August 11, 2009 and accepted October 27, 2009.

Published online November 4, 2009. 10.1021/nn900986r CCC: $40.75

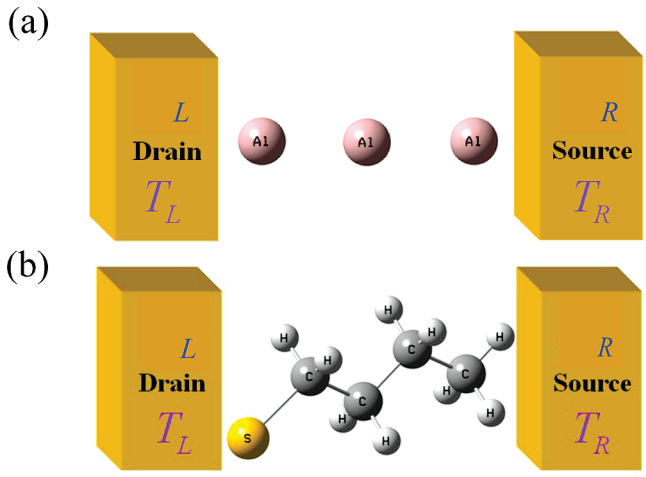

Scheme 1. Schemes of the systems investigated: (a) the 3-Al atomic junction and (b) the C_4 molecular junction. Two bulk electrodes are modeled as independent electron reservoirs with distinct chemical potentials $\mu_{L(R)}$ and distinct temperatures $T_{L(R)}$.

infinity, the thermoelectric efficiency of nanojunctions will reach the Carnot efficiency. To obtain a large ZT value, the thermoelectric nanojunction would need to have a large value of S, a large value of σ, and a small value of the combined heat conductance ($\kappa_{el} + \kappa_{ph}$). Thermoelectric devices with a large value of σ are usually accompanied by a large value of κ_{el}, owing to the same proportionality with the transmission function. In the case that $\kappa_{ph} \ll \kappa_{el}$, the cancelation between σ and κ_{el} makes the enhancement of the thermoelectric figure of merit ZT quite a challenging task.

Using the first-principles approaches, we investigate the fundamental properties of ZT in nanojunctions in this paper. We focus on small-sized atomistic systems wherein electron transport is essentially ballistic. The objective of this study is to obtain qualitative and quantitative descriptions of ZT for temperatures and lengths of the nanojunctions. As an example, we investigate ZT for aluminum (conducting) atomic junctions and alkanethiol (insulating) molecular junctions (see Scheme 1). The Al atomic junctions are ideal test beds for studying the charge transport in the ballistic system at the atom scale level.[16−19] In contrast to the conductor behavior of Al atomic junctions wherein the resonant tunneling is the major transport mechanism, alkanethiol molecular junctions serve as insulators. Alkanethiols [$CH_3(CH_2)_{n-1}SH$, denoted as C_n] are a good illustration of reproducible junctions that can be fabricated.[20,21] It has been established that nonresonant tunneling is the main conduction mechanism in alkanethiol junctions. Consequently, the conductance is small and decreases exponentially with the length of junction given as $\sigma = \sigma_0 \exp(-\xi l)$, where l is the length of junctions and $\xi \approx 0.78$ Å^{-1}. To obtain quantitative description of ZT for temperatures and lengths of the nanojunctions, the self-consistent density functional theory (DFT) in the scattering approaches has been performed. The effective single-particle wave functions have then been applied to calculate the electric conductance σ, the Seebeck coefficient S, and the electronic heat conductance κ_{el}. However, in the absence of the phononic heat conductance, the research on ZT is incomplete. In this study, we have considered the combined heat conductance including both electronic heat conductance and phononic heat conductance. To consider the phononic heat current, the macroscopic electrodes have been taken as ideal thermal conductors with distinct temperatures. The rate of thermal energy flow between two macroscopic temperature reservoirs joined by a nanostructured object has been then estimated by a weak link model equivalent to the thermal Landauer formula in the weak tunneling limit.[22] The weak mechanical link is then modeled by a harmonic spring of stiffness (K).

To gain further insights into the qualitative description of ZT on the dependence of the temperatures and lengths in the nanojunctions, we have developed an analytical theory for ZT. In the low-temperature regime with bias nearing zero, we have expanded the Seebeck coefficient S, the electronic heat conductance κ_{el}, and the phononic heat conductance κ_{ph} to the lowest order in temperatures. We have observed a characteristic temperature $T_0 = (\beta/\gamma(l))^{1/2}$, at which the electronic heat conductance equals the phononic heat conductance, that is, $\kappa_{el}(T_0) = \kappa_{ph}(T_0)$. For $T \ll T_0$, the combined heat conductance is dominated by the electronic heat conductance ($\kappa_{el}(T) \gg \kappa_{ph}(T)$), and it is found that ZT $\propto T^2$. For $T \gg T_0$, the combined heat conductance is dominated by the phononic heat conductance ($\kappa_{el}(T) \ll \kappa_{ph}(T)$), and it is found that ZT tends to a saturation value.

In addition, the relation between ZT and the junction lengths depends on the electron transport mechanism. For the alkanethiol (insulating) molecular junctions, the saturation value of ZT decreases as the length increases; on the other hand, for the aluminum (conducting) atomic junctions, the saturation value of ZT increases as the length increases. Different characteristics in ZT can be attributed to the difference in electron transport mechanisms between the Al atomic junctions and the C_n molecular junctions. For the C_n junctions, the electric conductance decreases exponentially [$\sigma = \sigma_0 \exp(-\xi l)$] due to the insulating behavior. Consequently, the length characteristic of ZT becomes dominated by the electric conductance [$\sigma \propto \exp(-\xi l)$], such that ZT decreases exponentially as the length increases. For Al atomic junctions, the electric conductances range from 1 to $2G_0$, which are relatively insensitive to the lengths compared with the C_n junctions, due to resonant tunneling. In this case, the length characteristic of ZT is dominated by the phononic heat conductance $\kappa_{ph} \propto l^{-2}$ when $T \gg T_0$; consequently, ZT increases as the lengths of junctions increase. For these reasons, the length-dependent characteristic of ZT for

the metallic atomic junctions becomes opposite to that of the insulating molecular junctions. Therefore, longer conducting atomic junctions and shorter insulating molecular junctions show better thermoelectric efficiency.

The nanojunction with a large Seebeck coefficient is of key importance in increasing ZT. The characteristic of such nanojunctions is a sharp peak around the Fermi levels in the DOS,[14] and the Seebeck coefficient can be further optimized by applying the gate field.[7,14] The widely diversified atomic-sized junctions may be achieved by manipulating the species of nanostructured objects and the contact region. Such manipulations may lead to a significant change in the density of states (DOSs), consequently varying the Seebeck coefficient of the nanojunctions. A full exploration of all possibilities in such an unknown system may lead to observations of the large ZT suitable for practical thermoelectric nanodevices. The results of this study may be of interest to researchers attempting to develop new styles of thermoelectric nanodevices.

The flow of the discussion for this paper is as follows. We present the analytical theory of ZT and comparative studies on ZT for the atomic junctions and molecular junctions of various lengths in Results and Discussion. We then summarize our findings in Conclusions. Finally, we describe the theory of first principles calculations for ZT in Theoretical Methods.

RESULTS AND DISCUSSION

We have performed first-principles calculations to investigate ZT in Al atomic junctions and C_n molecular junctions using eq 14 for the Seebeck coefficient, eq 15 for the electric conductance, eq 19 for the electronic heat conductance, and eq 23 for the phononic heat conductance. To gain further insights into the qualitative description of ZT on the dependence of the temperatures and lengths, we expand the Seebeck coefficient S, the electronic heat conductance κ_{el}, and the phononic heat conductance κ_{ph} to their lowest order in temperatures. Equations 14, 19, and 23 can then be described by the following power law expansions:

$$S \approx \alpha T \tag{2}$$

$$\kappa_{el} \approx \beta T \tag{3}$$

and

$$\kappa_{ph} \approx \gamma(l) T^3 \tag{4}$$

where $\alpha = -\pi^2 k_B^2 (\partial\tau(\mu)/\partial E)/(3e\tau(\mu))$, $\beta = 2\pi^2 k_B^2 \tau(\mu)/(3h)$, and $\gamma(l) = 8\pi^5 k_B^4 C^2 A^2 Y^2/(15\hbar l^2)$. Here $\tau(E)$ is the transmission function given by eq 11; μ is the chemical potential; Y is the Young's modulus of the junction; A (l) is the cross section (length) of the nanostructured object sandwiched between electrodes; and C is a constant, which is given by the spectral density of phonon states at the left (right) electrode surface: $N_{L(R)}(E) \simeq CE$.[23,24] As a consequence of eqs 2, 3, and 4, the thermoelectric figure of merit, $ZT = S^2\sigma T/(\kappa_{el} + \kappa_{ph})$, in the nanojunctions has a simple form

$$ZT \approx \frac{\alpha^2 \sigma T^3}{\beta T + \gamma(l) T^3} \rightarrow \begin{cases} (\alpha^2\sigma/\beta)T^2, \text{ for } T \ll T_0, \\ \alpha^2\sigma/\gamma(l), \text{ for } T \gg T_0, \end{cases} \tag{5}$$

which is valid in when $T_R \approx T_L = T$ and $V_B = 0$ V.

We observe a characteristic temperature, $T_0 = (\beta/\gamma(l))^{1/2}$, for ZT in the nanoscale junctions. The characteristic temperature, T_0, is defined as the temperature where the electronic heat conductance equals the phononic heat conductance, that is, $\kappa_{el}(T_0) = \kappa_{ph}(T_0)$ in small temperature regime. When $T \ll T_0$, where $\kappa_{ph}(T) \ll \kappa_{el}(T)$, the electronic heat conductance dominates the combined heat conductance, and ZT increases as the temperature increases: $ZT \approx \sigma S^2 T/\kappa_{el} \approx [\alpha^2\sigma/\beta]\, T^2$. Similarly, when $T \gg T_0$, where $\kappa_{ph}(T) \gg \kappa_{el}(T)$, the phononic heat conductance dominates the combined heat conductance, and ZT tends to a saturation value: $ZT \approx \sigma S^2 T/\kappa_{ph} \approx \alpha^2\sigma/\gamma(l)$.

To increase $ZT = S^2\sigma T/(\kappa_{el} + \kappa_{ph})$, it is necessary to increase the Seebeck coefficient S and the electric conductance σ, as well as to decrease the combined heat conductance ($\kappa_{el} + \kappa_{ph}$). The presence of the phononic heat current increases the combined heat conductance, thus suppressing the thermoelectric figure of merit ZT. We suggest that κ_{ph} be minimized ($\kappa_{ph} \rightarrow 0$) by choosing low elasticity bridging nanostructured object or by creating poor thermal contacts in the nanojunctions, while the electrons are still allowed to tunnel. In this case, $ZT \approx \sigma S^2 T/\kappa_{el}$. It is worth noting that σ and κ_{el} roughly cancel each other out in the contribution of ZT because both are proportional to $\tau(\mu)$. The cancelation between σ and κ_{el} makes the enhancement of ZT a challenging task.

In addition, it is noted that the phononic heat current dominates for $T \gg T_0$ where ZT tends to a saturation value ($ZT \rightarrow \sigma S^2 T/\kappa_{ph}$). The phononic heat conductance decreases as the length of nanojunction increases: $\kappa_{ph} \approx \gamma(l) T^3 \propto l^{-2}$. As a consequence, ZT increases as the length of the nanojunction increases in case that the σ is less sensitive to the length l such as the metallic atomic junctions. In contrast, the insulating molecular junctions show opposite trends. The electric conductance of insulating molecular junctions decreases exponentially with the length l [$\sigma = \sigma_0 \exp(-\xi l)$], which in turn, dominates the dependence of ZT on the length l. Therefore, the length characteristic of ZT for the metallic atomic junctions is opposite that of the insulating molecular junctions. For conducting atomic junctions, the saturation value of ZT increases as the length increases. On the other hand, for the insulating junctions, the saturation value of ZT decreases as the length increases. This point is explained using two catalogs of nanojunctions: the aluminum (conducting) atomic junc-

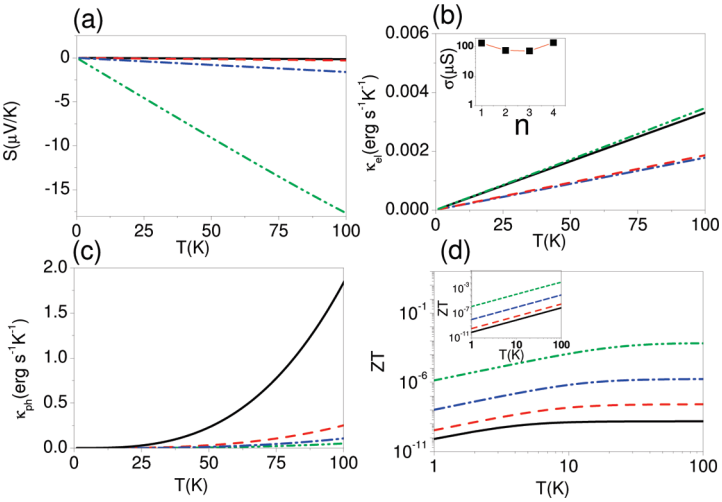

Figure 1. Aluminum atomic junctions at $V_B = 0$ V for 1 Al (solid black lines), 2 Al (dashed red lines), 3 Al (dot-dashed blue lines), and 4 Al (dot-dot-dashed green lines). (a) Seebeck coefficient S as a function of T. (b) Electronic heat conductance κ_{el} as a function of T. Inset shows semi-log of electric conductance σ as a function of the number of atoms. (c) Phononic heat conductance κ_{ph} as a function of T, (d) Log−log plot of ZT as a function of T. Inset shows the case of neglecting the phononic heat conductance $\kappa_{ph} = 0$.

tions and the alkanethiol (insulating) molecular junction, as discussed below.

Aluminum Atomic Junctions. Aluminum atomic junctions are ideal test beds to study the charge transport.[16−19] In order to investigate the length dependence of thermoelectric efficiency ZT, we study the Al atomic junctions for one to four atoms sandwiched between two bulk Al electrodes ($r_s \approx 2$). Figure 1a shows the Seebeck coefficient as a function of temperatures for various lengths of Al atomic junctions. The numerics show that the Seebeck coefficient is linear in temperatures, which corresponds well with the analytical expression in eq 2: $S \approx \alpha T$. At a fixed temperature, the magnitude of the Seebeck coefficient increases along with the increase of the number of Al atoms due to the corresponding increase of the slope in the transmission function at the Fermi level. As shown in the inset of Figure 1b, the electric conductance is relatively insensitive to the lengths of the junctions (typically around 1 to $2G_0$; $1G_0 \approx 77$ μS), apart from a possible four-atom periodicity due to a filling factor of 1/4 in the π orbital.[25] Meanwhile, as shown in the main body of Figure 1b, the magnitude of electronic heat conductance is linear in temperatures, which agrees well with eq 3: $\kappa_{el} \approx \beta T$. At a fixed temperature, the dependence of the magnitude of κ_{el} on the number of Al atoms is the same as that of σ, due to the fact that both σ and κ_{el} are proportional to the transmission function $\tau(\mu)$.

There is a characteristic temperature, T_0, defined as the temperature where $\kappa_{el}(T_0) = \kappa_{ph}(T_0)$. The numerics obtained from eqs 19 and 23 are given in Table 1, which agree well with the equation $T_0 = (\beta/\gamma(l))^{1/2}$ obtained from eqs 3 and 4 in the small temperature regime. The relation $T_0 = (\beta/\gamma(l))^{1/2}$ predicts that the characteristic temperatures increase as the lengths of aluminum atomic junction increase. The reason behind this is that the dependence of β on the lengths is weaker than that of γ ($\gamma(l) \propto l^{-2}$) in the Al metallic atomic junction.

TABLE 1. T_0 for Various Lengths of Al Atomic Junctions

nanojunctions	1 Al	2 Al	3 Al	4 Al
T_0(K)	4.2	8.6	12.9	23.1

Figure 1c shows the phononic heat conductance as a function of temperatures for various lengths of Al atomic chains, where the Young's modulus is given by $Y = 1.2 \times 10^{13}$ dyn/cm^2 from the total energy calculations.[23] The phononic heat conductance increases with T^3 as predicted in eq 4. As can be seen, when $T \gg T_0$, $\kappa_{ph} \gg \kappa_{el}$ is due to the large value of Young's modulus and the different temperature dependence for $\kappa_{el} \approx \beta T$ and $\kappa_{ph} \approx \gamma(l)T^3$. At a fixed temperature, κ_{ph} decreases as the length increases, which agrees well with the relation $\gamma(l) \propto l^{-2}$. Meanwhile, the main body of Figure 1d shows the thermoelectric figure of merit as a function of temperatures, where κ_{ph} is calculated using $Y = 1.2 \times 10^{13}$ dyn/cm^2 as the Young's modulus for the Al atomic junctions. The thermoelectric figure of merit reaches the saturation value, $ZT \rightarrow \alpha^2\sigma/\gamma(l)$ when $T \gg T_0$. The increase in the number of Al atoms sharply enhances the saturation value of ZT (approximately, $ZT \propto l^2S^2$) because of the increase in the Seebeck coefficient and the decrease of κ_{ph} ($\kappa_{ph} \propto l^{-2}$) by the lengths of the Al atomic junction. The mechanical elasticity of the Al junctions is sensitive to the detailed geometry in the contact region, which is unknown in the real experiment. If a mechanical link can be thwarted by creating a poor one while the electrons are still allowed to tunnel, then ZT could be strongly enhanced, as shown in the inset of Figure 1d, where the phononic heat conductance κ_{ph} is taken to be zero. In this case, the thermal current is only carried by electron transport so that $ZT \approx (\alpha^2\sigma/\beta)\,T^2$, and T_0 vanishes due to $\kappa_{ph} = 0$.

Alkanethiol Molecular Junctions. Alkanethiols [$CH_3(CH_2)_{n-1}SH$, denoted as C_n] are good examples of reproducible junctions that can be fabricated.[20,21] In contrast to the conductor behavior of aluminum atomic junctions, alkanethiol junctions serve as insulators. It has been established that nonresonant tunneling is the main conduction mechanism in alkanethiol junctions. Consequently, the conductance is small and decreases exponentially with the length of junction, as $\sigma = \sigma_0\exp(-\xi l)$, where l is the length of alkanethiol junction and $\xi \approx 0.78$ Å^{-1},[26−30] as shown in the inset of Figure 2b. The DFT calculations involve continuum states with large amount of energy mesh and a large basis over 3000 plane waves. Limited by the demanding computing resources, this study approximates the wave functions of the C_n junctions through a simple scaling factor exploiting the periodicity in the $(CH_2)_2$ group of the alkanethiol chains, which leads to exponential scal-

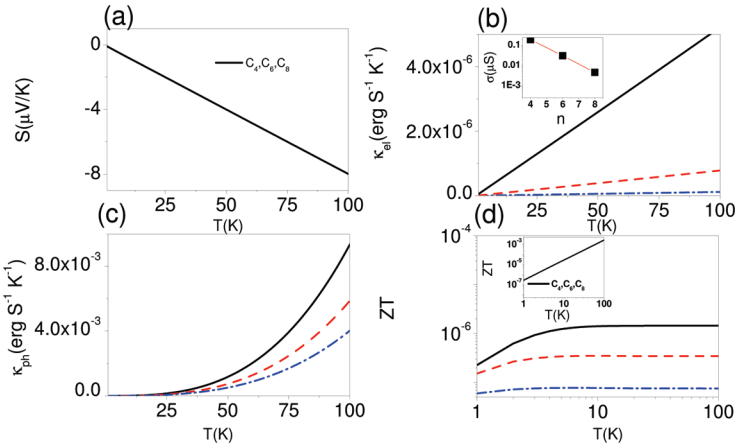

Figure 2. Alkanethiol junctions at $V_B = 0$ V for C_4 (solid black lines), C_6 (dashed red lines), and C_8 (dot-dashed lines). (a) Seebeck coefficient S as a function of T. (b) Electronic heat conductance κ_{el} as a function of T. Inset shows semi-log of electric conductance σ as a function of n, where n is the number of carbon atoms. (c) Phononic heat conductance κ_{ph} as a function of T. (d) Log−log of ZT as a function of T. Inset shows the case of neglecting of the phononic heat conductance $\kappa_{ph} = 0$.

ing in the transmission function $\tau(E)$. Meanwhile, Figure 2a shows the magnitude of the Seebeck coefficient as a function of temperatures for various C_n junctions. The Seebeck coefficient is linear in temperature as denoted in, $S \approx -[(\pi^2 k_B^2/3e\tau(\mu)) \cdot (\partial\tau(\mu)/\partial E)]T$, and its dependence on the number of carbon atoms is canceled due to the same scaling factor, $\exp(-\xi l)$, for both $\tau(\mu)$ and $\partial\tau(\mu)/\partial E$. We note that the cancelation may not be complete in the real experiments; thus, the Seebeck coefficient could possibly show weak length dependence due to other effects.[2,4]

As shown in the main body of Figure 2b, the magnitude of electronic heat conductance is linear in temperatures, $\kappa_{el} \approx \beta T$. At a fixed temperature, the magnitude of κ_{el} decreases exponentially with n, which is the number of carbon atoms in C_n, owing to the scaling behavior of $\tau(E)$. As shown in Figure 2c, phononic heat conductance increases as the temperature increases as denoted by $\kappa_{ph} = \gamma(l)T^3$ for the Young's modulus estimated by the total energy calculations.[24] At a fixed temperature, κ_{ph} decreases as n^{-2} due to $\gamma(l) \propto l^{-2}$ (see Figure 2c). Due to the small transmission probability for the insulating alkanethiol junctions, the electronic heat conductance (note, $\kappa_{el} \propto \sigma$) is much suppressed such that $\kappa_{el} \ll \kappa_{ph}$, as shown in Figure 2b,c.

The respective characteristic temperature, T_0, for various C_n junctions are listed in Table 2. The trend of the dependence of T_0 on lengths in C_n junctions is opposite to that in the aluminum atomic junctions. The reason is that the length characteristic of β in the C_n junctions decreases exponentially [as $\tau(\mu) \propto \exp(-\xi l)$], which is stronger than that of $\gamma(l) \propto l^{-2}$. Thus, the length characteristic of $T_0 \approx (\beta/\gamma(l))^{1/2}$ is dominated by $\beta \propto \exp(-\xi l)$. Consequently, the characteristic temperature, T_0, decreases as the lengths of C_n junctions increase. The T^2 regime for ZT (where $T \ll T_0$) is significantly suppressed owing to the insulating behavior of of the C_n junctions.

TABLE 2. T_0 for Various C_n Molecular Junctions

nanojunctions	C_4	C_6	C_8
T_0(K)	2.3	1.2	0.5

The main body of Figure 2d shows ZT as a function of temperatures for various C_n junctions. The thermoelectric figure of merit tends to a saturation value for $T \gg T_0$. The saturation values of ZT decrease as the lengths increase. Owing to the insulating behavior of C_n junctions, $ZT \approx \alpha^2\sigma/\gamma(l) \propto l^2\exp(-\xi l)$ because $\sigma \propto \exp(-\xi l)$, $\gamma(l) \propto l^{-2}$, and $\alpha \approx$ constant. Nevertheless, there is enough experimental evidence to show that the junctions have poor thermal contacts for certain samples.[31] Those samples quickly frustrate at much smaller biases due to poor heat dissipation when the local heating is triggered.[18,32,33] In such cases, the bridging nanostructure effectively has a very small Young's modulus. In the limit of extremely poor phononic thermal contacts (effectively, $\kappa_{ph} = 0$), which leads to $ZT \propto \alpha^2\sigma T^2/\beta$. It implies that ZT is not affected by the lengths of C_n junctions [noting that $\sigma \propto \exp(-\xi l)$ and $\beta \propto \exp(-\xi l)$ cancels the length dependence], as shown in the inset of Figure 2d. The cancelation may not be complete in the real experiments, and as such, ZT could possibly show weak length dependence due to other effects.

CONCLUSIONS

In conclusion, the self-consistent DFT calculations together with analytical expressions are applied to investigate the thermoelectric figure of merit ZT in the nanoscale junctions. There is a characteristic temperature T_0 for ZT, which is defined as the temperature where the electronic heat conductance equals the phononic heat conductance. When $T \ll T_0$, the electronic heat conductance dominates the combined heat conductance and $ZT \propto (\alpha^2\sigma/\beta)T^2$; when $T \gg T_0$, the phononic heat conductance dominates the combined heat conductance and ZT trends to the saturation value $\alpha^2\sigma/\gamma(l)$.

The relation between ZT and the lengths of nanojunction depends on the conducting mechanism: for aluminum (conducting) atomic junctions, the saturation value of ZT increases as the length increases because $\kappa_{ph} \propto l^{-2}$ dominates the length dependence; while for the alkanethiol (insulating) chains, the saturation value of ZT decreases as the length increases, owing to $\propto \exp(-\xi l)$, which dominates the length dependence. Thus, the dependence of ZT on the lengths for

the metallic atomic junctions is opposite to that for the insulating molecular junctions. In addition, we also find that T_0 of the aluminum (conducting) atomic junction increases as the length of the junction increases; on the other hand, T_0 of the alkanethiol (insulating) junction decreases as the length of the junction increases. The difference in the length dependence between the insulating molecular junctions and the metallic atomic junctions is due to different length-scaling behavior in the electric conductance.

Of key importance to increasing the thermoelectric efficiency is using materials with a large value of Seebeck coefficient. Such materials are usually characterized by a sharp peak in the transmission function near the Fermi levels. The thermoelectric efficiency could be further optimized by applying gate fields or choosing low-elasticity bridging materials in nanoscale junctions. The widely diversified atomic-sized junctions may be achieved by manipulating the species of nanostructured objects and the contact region. Such manipulations may lead to a significant change in DOSs, consequently varying the Seebeck coefficient of the nanojunctions. A full exploration of all the possibilities in such an unknown system may lead to observations of large ZT values, suitable for practical thermoelectric nanodevices. The conclusions of this study may be beneficial to further studies attempting to increase the thermoelectric efficiency through the design of thermoelectric nanodevices at the atomic and molecular levels.

THEORETICAL METHODS

In the subsection Density Functional Theory, we present an introduction to the density functional theory (DFT) in the scattering approaches. In the subsection Theory of ZT, we briefly introduce the method of applying DFT to compute the electric conductance σ, the Seebeck coefficient S, and the electronic heat conductance κ_{el}. We also briefly introduce the method to calculate the phononic heat conductance κ_{ph} from the weak link model.[22]

Density Functional Theory. We start with a brief introduction of how to calculate the electric current and the electronic heat current carried by the electron transport in the DFT framework. We picture a nanoscale junction as formed by two semi-infinite electrodes held a fixed distance apart, with a nanostructured object bridging the gap between them. The full Hamiltonian of the system is $H = H_0 + V$, wherein H_0 is the Hamiltonian due to the bare electrodes, and V is the scattering potential of the nanostructured object. The nanostructured object could be a single atom, a chain of atoms, a molecule, or any system with nanoscale dimension. First, we calculate the wave functions of the bare electrodes with an applied bias $V_B = (\mu_R - \mu_L)/e$, where $\mu_{L(R)}$ is the chemical potential deep in the left (right) electrode. The unperturbed wave functions of the bare electrodes have the form, $\Psi^{0,L(R)}_{E\mathbf{K}_\parallel}(\mathbf{r}) = e^{i\mathbf{K}_\parallel\cdot\mathbf{R}}\cdot u^{L(R)}_{E\mathbf{K}_\parallel}(z)$, where $u^{L(R)}_{E\mathbf{K}_\parallel}(z)$ describes the electrons incident from the left (right) electrode before the inclusion of the nanostructured object. The equation $u^{L(R)}_{E\mathbf{K}_\parallel}(z)$ is calculated by solving the Shrödinger equation and Poisson equation iteratively until self-consistency is obtained. We note that $u^{R}_{E\mathbf{K}_\parallel}(z)$ satisfies the following boundary condition:

$$u^{R}_{E\mathbf{K}_\parallel}(z) = (2\pi)^{-3/2}\times\begin{cases}\dfrac{1}{\sqrt{k_R}}(e^{-ik_Rz} + Re^{ik_Rz}), z\to\infty,\\ \dfrac{1}{\sqrt{k_L}}Te^{-ik_Lz}, z\to-\infty,\end{cases} \quad (6)$$

where $\mathbf{K}_\parallel$ is the electron momentum in the plane parallel to the electrode surfaces, and z is the coordinate parallel to the current's direction. The condition of energy conservation gives $1/2k_R^2 = E - 1/2|\mathbf{K}_\parallel|^2 - v_{eff}(\infty)$ and $1/2k_L^2 = E - 1/2|\mathbf{K}_\parallel|^2 - v_{eff}(-\infty)$, wherein $v_{eff}(z)$ is the effective potential comprising the electrostatic potential and the exchange-correlation potential.

The nanostructured object is considered in the scattering approaches. The scattering wave functions of the entire system are calculated by solving the Lippmann−Schwinger equation iteratively until self-consistency is obtained

$$\Psi^{L(R)}_{E\mathbf{K}_\parallel}(\mathbf{r}) = \Psi^{0,L(R)}_{E\mathbf{K}_\parallel}(\mathbf{r}) + \int d^3\mathbf{r}_1\int d^3\mathbf{r}_2 G^0_E(\mathbf{r},\mathbf{r}_1)V(\mathbf{r}_1,\mathbf{r}_2)\Psi^{L(R)}_{E\mathbf{K}_\parallel}(\mathbf{r}_2) \quad (7)$$

where $\Psi^{L(R)}_{E\mathbf{K}_\parallel}(\mathbf{r})$ stands for the effective single-particle wave functions of the entire system, which also represents the electrons with energy E incident from the left (right) electrode. The potential $V(\mathbf{r}_1,\mathbf{r}_2)$ the electrons experience when they scatter through the nanojunction is

$$V(\mathbf{r}_1,\mathbf{r}_2) = V_{ps}(\mathbf{r}_1,\mathbf{r}_2) + \left\{V_{xc}[n(\mathbf{r}_1)] - V_{xc}[n_0(\mathbf{r}_1)] + \int d\mathbf{r}_3\frac{\delta n(\mathbf{r}_3)}{|\mathbf{r}_1-\mathbf{r}_3|}\right\} \quad (8)$$

where $V_{ps}(\mathbf{r}_1,\mathbf{r}_2)$ is the electron−ion interaction potential represented with pseudopotential; $V_{xc}[n(\mathbf{r}_1)]$ is the exchange-correlation potential calculated at the level of the local-density approximation; $n_0(\mathbf{r})$ is the electron density for the pair of biased bare electrodes; $n(\mathbf{r})$ is the electron density for the total system; and $\delta n(\mathbf{r})$ is their difference. The quantity G^0_E is the Green's function for the bare electrodes. A basis of about 3000 plane waves has been chosen for this study. The wave functions that achieve self-consistency in the DFT framework are applied to calculate the electric current, the Seebeck coefficient, and the electronic heat current carried by the electrons.

These right- and left-moving wave functions, weighting with the Fermi-Dirac distribution function according to their energies and temperatures, are applied to calculate the electric current as

$$I = \frac{e\hbar}{mi}\int dE\int d\mathbf{R}\int d\mathbf{K}_\parallel\left(f^R_E\cdot\mathbf{I}^{RR}_{EE,\mathbf{K}_\parallel} - f^L_E\cdot\mathbf{I}^{LL}_{EE,\mathbf{K}_\parallel}\right) \quad (9)$$

where $I^{RR(LL)}_{EE,\mathbf{K}_\parallel} = [\Psi^{R(L)}_{E,\mathbf{K}_\parallel}]^*\nabla\Psi^{R(L)}_{E,\mathbf{K}_\parallel} - \nabla[\Psi^{R(L)}_{E,\mathbf{K}_\parallel}]^*\Psi^{R(L)}_{E,\mathbf{K}_\parallel}$ and $d\mathbf{R}$ represents an element of the electrode surface. Here we have assumed that the left and right electrodes are independent electron reservoir, with the electron population described by the Fermi Dirac distribution function, $f^{L(R)}_E = 1/(\exp((E-\mu_{L(R)})/k_BT_{L(R)}) + 1)$, where $\mu_{L(R)}$ and $T_{L(R)}$ are the chemical potential and the temperature in the left (right) electrode, respectively. More detailed descriptions of theory can be found in refs 34−36.

The above expression can be casted into a Landauer−Büttiker formalism:

$$I = \frac{2e}{h}\int dE[f^R_E(\mu_R,T_R) - f^L_E(\mu_L,T_L)]\tau(E) \quad (10)$$

where $\tau(E) = \tau^R(E) = \tau^L(E)$ is a direct consequence of the time-reversal symmetry, and $\tau^{R(L)}(E)$ is the transmission function of the electron with energy E incident from the right (left) electrode

$$\tau^{R(L)}(E) = \frac{\pi\hbar^2}{mi}\int d\mathbf{R}\int d\mathbf{K}_\parallel I^{RR(LL)}_{EE,\mathbf{K}_\parallel}(\mathbf{r}) \quad (11)$$

Theory of ZT. In this subsection, we briefly describe the method used to calculate the Seebeck coefficient S, the electric conductance σ, and the electronic heat conductance κ_{el}. We also describe the method to calculate the phononic heat conductance κ_{ph} *via* the weak link model.

We begin with the description of the method for the calculation of the Seebeck coefficient. We assume that the left (right) electrode serves as the electron and thermal reservoir with the electron population described by the Fermi-Dirac distribution function. We consider an extra current induced by an additional infinitesimal temperature (ΔT) and voltage (ΔV) distributed symmetrically across the junctions

$$\Delta I = I\left(\mu_L, T_L + \frac{\Delta T}{2}; \mu_R, T_R - \frac{\Delta T}{2}\right) + I\left(\mu_L + \frac{e\Delta V}{2}, T_L; \mu_R - \frac{e\Delta V}{2}, T_R\right) - 2I(\mu_L, T_L; \mu_R, T_R) \quad (12)$$

After expanding the Fermi-Dirac distribution function to the first order in ΔT and ΔV, we obtain the Seebeck coefficient (defined by $S = \Delta V/\Delta T$) by letting $\Delta I = 0$

$$S = -\frac{1}{e}\frac{\frac{K_1^L}{T_L} + \frac{K_1^R}{T_R}}{K_0^L + K_0^R} \quad (13)$$

where $K_n^{L(R)} = -\int dE(E - \mu_{L(R)})^n[\partial f_E^{L(R)}/\partial E]\tau(E)$, and $\tau(E) = \tau^R(E) = \tau^L(E)$. In this paper, we focus on the zero bias regime with two electrodes at the same temperatures ($\mu_L = \mu_R = \mu$; $T_L = T_R = T$); eq 13 above can be simplified as

$$S = -\frac{1}{eT}\frac{\int (E - \mu)\frac{\partial f_E}{\partial E}\tau(E)dE}{\int \frac{\partial f_E}{\partial E}\tau(E)dE} \quad (14)$$

In addition, the differential conductance, typically not sensitively related to temperatures in cases where direct tunneling is the major transport mechanism, may be expressed as

$$\sigma = \frac{2e^2}{h}\int\left(-\frac{\partial f_E}{\partial E}\right)\tau(E)dE \quad (15)$$

Second, the electronic heat current, which removes the thermal energy from the left (right) temperature reservoirs, is expressed by

$$J_{el}^{L(R)} = \frac{2}{h}\int dE\{[E - \mu_{L(R)}][f_E^{R(L)}(E) - f_E^{L(R)}(E)]\tau(E)\} \quad (16)$$

Near the zero bias ($\mu_L \approx \mu_R = \mu$), we note that $J_{el}^L = -J_{el}^R = J_{el}$, and as such, eq 16 can be written as

$$J_{el} = \frac{2}{h}\int dE\{(E - \mu)[f_E^R(E) - f_E^L(E)]\tau(E)\} \quad (17)$$

Considering an extra thermal current induced by an additional infinitesimal temperature (ΔT) and voltage (ΔV) symmetrically distributed across the junction, we come up with

$$\Delta J_{el} = J_{el}\left(\mu, T + \frac{\Delta T}{2}; \mu, T - \frac{\Delta T}{2}\right) + J_{el}\left(\mu + \frac{e\Delta V}{2}, T; \mu - \frac{e\Delta V}{2}, T\right) \quad (18)$$

We obtain the electronic heat conductance (defined by $k_{el} = \Delta J_{el}/\Delta T$) after expanding the Fermi-Dirac distribution function to the first order in ΔT and ΔV expressed by

$$\kappa_{el} = \frac{2}{h}\left[K_1 eS + \frac{K_2}{T}\right] \quad (19)$$

where $K_n = -\int dE(E - \mu)^n[\partial f_E/\partial E]\tau(E)$. Thus far, the physical quantities (S, σ, and κ_{el}) previously discussed are related to the propagation of electrons. However, it must be noted that the heat current can be conveyed by the propagation of electrons and phonons. In the absence of the phononic heat conductance, the research on ZT is incomplete. As such, in order to consider the phonon contribution to ZT, it is assumed that the nanojunction is a weak elastic link, with a given stiffness K that we evaluate from total energy calculations. Two metal electrodes are regarded as the macroscopic bodies under their thermodynamic equilibrium and are taken as ideal thermal conductors. To leading order in the strength of the weak link, the mechanical link is modeled by a harmonic spring. We then estimate the phononic heat current (J_Q^{ph}) *via* elastic phonon scattering as[22]

$$J_Q^{ph} = \frac{2\pi K^2}{\hbar}\int_0^\infty dEEN_L(E)N_R(E)[n_L(E) - n_R(E)] \quad (20)$$

where the stiffness $K = AY/l$ is evaluated from the first-principles.[23,24] The symbol, Y, is the Young's modulus of the junction, and A (l) is the cross section (length) of the nanostructured object sandwiched between electrodes. $N_{L(R)}(E) \simeq CE$, where C is a constant, is the spectral density of phonon states at the left (right) electrode surface.[37] Here, we have assumed that the metal electrodes are thermodynamically in equilibrium as described by the Bose−Einstein distribution function $n_{L(R)} \equiv 1/(e^{E/K_BT_{L(R)}} - 1)$. The rate of thermal energy carried by phonons flowing between two bulk electrodes joined by a nanostructured object is appropriately considered in the weak link model, which is valid for temperatures lower than the Debye temperatures.[22] The range of temperatures in the current study lies within this region (the Debye temperature is 394 K for Al and 170 K for Au). The phononic heat conductance is defined as

$$\kappa_{ph} = \left[J_Q^{ph}\left(T_L + \frac{\Delta T}{2}, T_R - \frac{\Delta T}{2}\right) - J_Q^{ph}(T_L, T_R)\right]/\Delta T \quad (21)$$

After expanding the Bose−Einstein distribution function in the left (right) electrode to the first order of ΔT in the expression of the phononic heat current, the phononic heat conductance is thus obtained:

$$\kappa_{ph} = \frac{\pi K^2 C^2}{\hbar}\int_0^\infty dEE^3\sum_{i=L,R}\frac{\partial n_i(E)}{\partial T_i} \quad (22)$$

When $T_R \approx T_L = T$, then eq 22 can be written as

$$\kappa_{ph} = \frac{2\pi K^2 C^2}{\hbar}\int_0^\infty dEE^3\frac{\partial n(E)}{\partial T} \quad (23)$$

where $n = 1/[e^{E/(k_BT)} - 1]$. Finally, when $\mu_L \approx \mu_R = \mu$ and $T_R \approx T_L = T$, the thermoelectric figure of merit $ZT = S^2\sigma T/(\kappa_{el} + \kappa_{ph})$ can be calculated using eqs 14, 15, 19, and 23.

Acknowledgment. The authors thank Professors N. J. Tao and Barry D. Dunietz for inspiring discussions. The authors thank MOE ATU, NCTS, and NCHC for support under Grants NSC 97-2112-M-009-011-MY3, 097-2816-M-009-004, and 97-2120-M-009-005.

REFERENCES AND NOTES

1. Ludoph, B.; van Ruitenbeek, J. M. Thermopower of Atomic-Size Metallic Contacts. *Phys. Rev. B* **1999**, *59*, 12290–12293.
2. Reddy, P.; Jang, S. Y.; Segalman, R. A.; Majumdar, A. Thermoelectricity in Molecular Junctions. *Science* **2007**, *315*, 1568–1571.
3. Baheti, K.; Malen, J. A.; Doak, P.; Reddy, P.; Jang, S. Y.; Tilley, T. D.; Majumdar, A.; Segalman, R. A. Probing the Chemistry of Molecular Heterojunctions Using Thermoelectricity. *Nano Lett.* **2008**, *8*, 715–719.
4. Malen, J. A.; Doak, P.; Baheti, K.; Tilley, T. D.; Segalman, R. A.; Majumdar, A. Identifying the Length Dependence of Orbital Alignment and Contact Coupling in Molecular Heterojunctions. *Nano Lett.* **2009**, *9*, 1164–1169.
5. Paulsson, M.; Datta, S. Thermoelectric Effect in Molecular Electronics. *Phys. Rev. B* **2003**, *67*, 241403(R).
6. Zheng, X.; Zheng, W.; Wei, Y.; Zeng, Z.; Wang, J. Thermoelectric Transport Properties in Atomic Scale Conductors. *J. Chem. Phys.* **2004**, *121*, 8537–8541.

7. Wang, B.; Xing, Y.; Wan, L.; Wei, Y.; Wang, J. Oscillatory Thermopower of Carbon Chains: First-Principles Calculations. *Phys. Rev. B* **2005**, *71*, 233406.
8. Galperin, M.; Nitzan, A.; Ratner, M. A. Inelastic Effects in Molecular Junction Transport: Scattering and Self-Consistent Calculations for the Seebeck Coefficient. *Mol. Phys.* **2008**, *106*, 397–404.
9. Pauly, F.; Viljas, J. K.; Cuevas, J. C. Length-Dependent Conductance and Thermopower in Single-Molecule Junctions of Dithiolated Oligophenylene Derivatives: A Density Functional Study. *Phys. Rev. B* **2008**, *78*, 035315.
10. Finch, C. M.; García-Suárez, V. M.; Lambert, C. J. Giant Thermopower and Figure of Merit in Single-Molecule Devices. *Phys. Rev. B* **2009**, *79*, 033405.
11. Markussen, T.; Jauho, A. P.; Brandbyge, M. Electron and Phonon Transport in Silicon Nanowires: Atomistic Approach to Thermoelectric Properties. *Phys. Rev. B* **2009**, *79*, 035415.
12. Dubi, Y.; Di Ventra, M. Thermoelectric Effects in Nanoscale Junctions. *Nano Lett.* **2009**, *9*, 97–101.
13. Ke, S. H.; Yang, W.; Curtarolo, S.; Baranger, H. U. Thermopower of Molecular Junctions: An *Ab Initio* Study. *Nano Lett.* **2009**, *9*, 1011–1014.
14. Liu, Y. S.; Chen, Y. C. Seebeck Coefficient of Thermoelectric Molecular Junctions: First-Principles Calculations. *Phys. Rev. B* **2009**, *79*, 193101.
15. Liu, Y. S.; Chen, Y. C. Atomistic Thermoelectric Refrigerator: A Proposal *via* a First-Principles Calculation. cond-mat/arXiv:0908.0992, **2009**.
16. Lang, N. D.; Avouris, Ph. Oscillatory Conductance of Carbon-Atom Wires. *Phys. Rev. Lett.* **1998**, *81*, 3515–3518.
17. Kobayashi, N.; Brandbyge, M.; Tsukada, M. First-Principles Study of Electron Transport through Monatomic Al and Na Wires. *Phys. Rev. B* **2000**, *62*, 8430–8437.
18. Yang, Z.; Chshiev, M.; Zwolak, M.; Chen, Y. C.; Di Ventra, M. Role of Heating and Current-Induced Forces in the Stability of Atomic Wires. *Phys. Rev. B* **2005**, *71*, 041402(R).
19. Cuevas, J. C.; Levy Yeyati, A.; Martín-Rodero, A.; Bollinger, G. R.; Untiedt, C.; Agraït, N. Evolution of Conducting Channels in Metallic Atomic Contacts under Elastic Deformation. *Phys. Rev. Lett.* **1998**, *81*, 2990–2993.
20. Wang, W.; Lee, T.; Reed, M. A. Mechanism of Electron Conduction in Self-Assembled Alkanethiol Monolayer Devices. *Phys. Rev. B* **2003**, *68*, 035416.
21. Tao, N. J. Electron Transport in Molecular Junctions. *Nat. Nanotechnol.* **2006**, *1*, 173–181.
22. Patton, K. R.; Geller, M. R. Thermal Transport through a Mesoscopic Weak Link. *Phys. Rev. B* **2001**, *64*, 155320.
23. The aluminum junction consists of an Al atomic chain sandwiched between two Al electrodes modeled as electron jellium with $r_s \approx 2$. The following parameters have been used for the junctions: the Al−jellium distance is about 2.0 au; the Al−Al bond distances are 6.8, 6.3, and 5.8 au for 2-Al, 3-Al, and 4-Al wires, respectively; the effective cross section chosen is $A = 23.1$ au^2 for the aluminum junction; the spectral densities of electrodes are evaluated using the longitudinal and transverse sound velocities for Al, $v_l = 6.35 \times 10^5$ cm/s and $v_t = 3.1 \times 10^5$ cm/s, respectively; the Young's modulus of aluminum junction, $Y \simeq 1.2 \times 10^{13}$ dyn/cm^2, has been calculated by total energy calculations for an atomic chain in perfect alignment. The Young's modulus has been found to be almost independent of the length of the junctions. We note that the value of the Young's modulus may be overestimated in comparison with real experiments where the geometry of the atom chain may be zigzag.
24. The arlkanethiol junction consists of a C_4 molecule sandwiched between two Au electrodes modeled as electron jellium with $r_s \approx 3$. The structure of the C_4 molecule has been relaxed using Gaussian03. The Au−jellium distance is set to be one half of the spacing between atom planes in (1,1,1) direction (see ref 30 for detailed description). The following parameters were used for the junctions: the effective cross section chosen is 21.4 au^2 for alkanethiol junction; the spectral densities of electrodes have been evaluated using the longitudinal and transverse sound velocities for Au, $v_l = 3.2 \times 10^5$ cm/s and $v_t = 1.2 \times 10^5$ cm/s, respectively; the Young's modulus of alkanethiol junction, $Y \simeq 2.3 \times 10^{12}$ dyn/cm^2, has been calculated by total energy calculations.
25. Thygesen, K. S.; Jacobsen, K. W. Conduction Mechanism in a Molecular Hydrogen Contact. *Phys. Rev. Lett.* **2005**, *94*, 036807.
26. Wold, D. J.; Frisbie, C. D. Fabrication and Characterization of Metal−Molecule−Metal Junctions by Conducting Probe Atomic Force Microscopy. *J. Am. Chem. Soc.* **2001**, *123*, 5549–5556.
27. Beebe, J. M.; Engelkes, V. B.; Miller, L. L.; Frisbie, C. D. Contact Resistance in Metal−Molecule−Metal Junctions Based on Aliphatic SAMs: Effects of Surface Linker and Metal Work Function. *J. Am. Chem. Soc.* **2002**, *124*, 11268–11269.
28. Zhao, J.; Uosaki, K. Formation of Nanopatterns of a Self-Assembled Monolayer (SAM) within a SAM of Different Molecules Using a Current Sensing Atomic Force Microscope. *Nano Lett.* **2002**, *2*, 137–140.
29. Kaun, C. C.; Guo, H. Resistance of Alkanethiol Molecular Wires. *Nano Lett.* **2003**, *3*, 1521–1525.
30. Ma, C. L.; Nghiem, D.; Chen, Y. C. Alkanethiol-Based Single-Molecule Transistors. *Appl. Phys. Lett.* **2008**, *93*, 222111.
31. Smit, R. H. M.; Untiedt, C.; van Ruitenbeek, J. M. The High-Bias Stability of Monatomic Chains. *Nanotechnology* **2004**, *15*, S472–S478.
32. Chen, Y. C.; Zwolak, M.; Di Ventra, M. Local Heating in Nanoscale Conductors. *Nano Lett.* **2003**, *3*, 1691–1694.
33. Chen, Y. C.; Zwolak, M.; Di Ventra, M. Inelastic Current−Voltage Characteristics of Atomic and Molecular Junctions. *Nano Lett.* **2004**, *4*, 1709–1712.
34. Lang, N. D. Resistance of Atomic Wires. *Phys. Rev. B* **1995**, *52*, 5335–5342.
35. Di Ventra, M.; Lang, N. D. Transport in Nanoscale Conductors from First Principles. *Phys. Rev. B* **2001**, *65*, 045402.
36. Chen, Y. C.; Di Ventra, M. Effect of Electron-Phonon Scattering on Shot Noise in Nanoscale Junctions. *Phys. Rev. Lett.* **2005**, *95*, 166802.
37. The value of C is 1.07×10^9 cm^2/erg^2 for Au electrodes and is 4.93×10^8 cm^2/erg^2 for Al electrodes. More detailed descriptions can be found in ref 22.